Scientia Iranica A (2012) 19 (5), 1220–1235

Sharif University of Technology

Scientia Iranica

Transactions A: Civil Engineering

www.sciencedirect.com

Effects of loading rate and initial stress state on stress–strain behavior of rock fill materials under monotonic and cyclic loading conditions

A. Aghaei Araei [a,*], H.R. Razeghi [b], A. Ghalandarzadeh [c], S. Hashemi Tabatabaei [a]

[a] *Department of Geotechnical Engineering, Road, Housing and Urban Development Research Center (BHRC), Tehran, P.O. Box: 13145-1696, Iran*
[b] *School of Civil Engineering, Iran University of Science and Technology, Tehran, P.O. Box: 16765-163, Iran*
[c] *Department of Civil Engineering, University of Tehran, Tehran, P.O. Box: 11365-4563, Iran*

Received 10 January 2012; revised 16 March 2012; accepted 1 August 2012

KEYWORDS

Spring;
Rubber;
Rockfill;
Triaxial;
Monotonic;
Cyclic;
Frequency;
Anisotropy;
Modulus;
Damping.

Abstract This paper studies loading rate effect on stress–strain behaviors of high compacted rockfill materials. The large scale triaxial-dynamic equipment was used for this propose. To check the equipment capabilities, tests have been carried out on elastic spring and damping rubber specimens. The laboratory tests results indicate that the loading rate effect in elastic metal spring is negligible, while it has considerable effects on stress–strain behaviors in damping rubber, and especially in rockfill materials. The laboratory test results on rockfill materials have shown that dry specimens have higher E and D values compared to the saturated samples. Anisotropic specimens have higher Young's modulus and less damping ratio in comparison to isotropic samples. Generally, the influence of the main parameters on E and D in rockfill specimens is initial vertical effective stress and loading frequency, respectively. The high compacted rockfill specimen exhibits a non-destructive response to the application of cyclic loading below a threshold axial strain level of $<0.005\%$. Since the frequency effect was observed in the strain levels lower than 0.005%, and there is not meaningful build up of pore pressure in this strain level, therefore any effect of excess pore water pressure on the frequency effect is negligible.

1. Introduction

Damping rubber and rockfill materials have many useful applications in civil engineering structures. For example, the damping rubber used as elastomeric bearing for seismic isolation of structures and bridges. Generally, damping rubber exhibits both nonlinear and viscous properties. Effects of temperature [1], strain amplitude [2] and strain rate [3] on modulus and damping ratio of damping rubber at strain higher than 5% were investigated previously. Moreover, modulus and damping ratio decrease as temperature and strain increase, whilst damping ratio and especially modulus increase as strain rate increases.

Furthermore, gravelly materials that have higher damping ratio compared to clay and sand materials are frequently used in the earth fill structures and rockfill dams. The seismic design of these structures at earthquake-prone regions requires determination of the stress–strain properties under monotonic and cyclic loading conditions of the used materials. The strength and deformation behavior of coarse granular media under monotonic condition were studied previously [4–7].

Over the past two decades, many investigators published cyclic triaxial shear test results for gravels [8–20]. In general, in cyclic loading using triaxial equipment, each stress–strain curve, which is named hysteresis loop, can be described by Young modulus (E) and damping ratio (D) curves. The word hysteresis comes from ancient Greek and means "lag" or "delay"; the time lag between a driven cyclic stress and the driving cyclic strain.

Many researchers [21,22] have shown that the dynamic properties of soils cannot be considered frequency independent in the earthquake frequency bandwidth, 0.01–30 Hz [23], even

* Corresponding author. Tel.: +98 21 88255942x260.
E-mail addresses: aghaeiaraei@bhrc.ac.ir (A. Aghaei Araei), razeghi@iust.ac.ir (H.R. Razeghi), aghaland@ut.ac.ir (A. Ghalandarzadeh), htabatabaei@bhrc.ac.ir (S. Hashemi Tabatabaei).

Peer review under responsibility of Sharif University of Technology.

Production and hosting by Elsevier

1026-3098 © 2012 Sharif University of Technology. Production and hosting by Elsevier B.V. Open access under CC BY-NC-ND license.
doi:10.1016/j.scient.2012.08.002

Nomenclature

The following symbols are used in this paper:

Ave.	Average
B_g	Marsal's Breakage index
c	Cohesion
$c_{c(\text{soil})}$	Critical damping of the soil specimen
c_{soil}	Viscous damping of the soil specimen
CD	Consolidated Drained
CFRDs	Concrete Faced Rockfill Dams
D	Damping ratio
D_{10}	Damping ratio at 10th cycle
$D_{(10)}, D_{(30)}, D_{(50)}, D_{(85)}$ (mm)	Particle size (mm) corresponding to 10, 30, 50 and 85 passing percentage, respectively
D_{40}	Damping ratio at 40th cycle
D_r	Relative density
e	Void ratio
e_o	Void ratio according to modified proctor compaction
e_i	Void ratio at end of consolidation
e_v	Volumetric strain
$e_{v(q_{\max})}$	Volumetric strain at the strain corresponding to the maximum deviator stress
ε_1	Major principal strain
E	Young's modulus
E_{10}	Modulus E at 10th cycle
E_{40}	Modulus E at 40th cycle
$E_{\max}$	Maximum value of Young's modulus
EPWP	Excess Pore Water Pressure
ϕ'	Effective friction angle at maximum shear stress
f	Frequency of the cyclic loading
$f_{n(\text{spring})}$	Natural frequency of the spring
f_{ns}	Natural frequency of the soil specimen in the free vibration
f_{ms}	Frequency at maximum amplitude (the resonant frequency) under cyclic loading of the soil specimen
F_0	Maximum amplitude of the cyclic loading
Hz	Hertz
I_s	Point Load Index
γ_d	Dry density
G	Shear modulus
G_s	Specific gravity
$k_c = \sigma_1'/\sigma_3'$	Initial stress conditions before cyclic loading
k_{soil}	Stiffness of the soil specimen
k_{spring}	Stiffness of the spring
l	Length of the spring
LA	Los Angeles Abrasion
L.B.	Lower bound
m_{cap}	Mass of the cap
m_{eff}	Effective mass $= m_{\text{cap}} + m_{\text{soil}}/3$
m_{soil}	Mass of the soil specimen
m_{spring}	Mass of the spring
P_h	Measured horizontal stresses at a point
P_v	Measured vertical stress at a point
$q = \sigma_1' - \sigma_3'$	Deviator stress
$q_{\max}$	Maximum deviator stress
SDOF	Single degree of freedom
σ_1'	Effective major principal stress
σ_3'	Effective minor principal stress, Effective confining pressure
$\sigma_m' = (\sigma_1' + 2\sigma_3')/3$	Mean effective stress
t	Time
T	Kinetic energy of the spring
U.B.	Upper bound
$U_{\max}$	Maximum accumulated excess pore water pressure at the end of the …th cycle
W_{opt}	Optimum water content
$\dot{z}$	Velocity of the top part of spring,
$\dot{z}_y$	Velocity of the spring element a distance y from the fixed end

for low strain level excitations [24] as it is common practice in geotechnical engineering [25]. Generally, the higher modulus is obtained from Resonant Column and Bender Element tests compared to triaxial and torsional shear tests. This may be due to higher loading frequency effect. Frequency effect on damping is not observed in triaxial and torsional shear element tests in previous research and can be explained as follows: most element tests are performed at very low frequencies of less than 1 Hz. In this range, perhaps the effect of frequency is negligible except for a creep effect which may be observed at a very low frequency. Generally, in Resonant Column test, damping is measured under free vibrations. It not necessary that the behavior of the material should be the same under free and forced vibrations and the material in forced vibration might not dissipate energy as expected according to the minimum principle. Recent test results show high damping ratio even at low strain levels ($<0.001\%$) in non Resonant Column tests [21,24]. Besides, higher damping ratio was observed at the resonant frequency [21]. Loading frequency and waveform effects on modulus and damping ratio of the three high compacted modeled rockfill materials were studied by means of a large scale triaxial testing [19]. The laboratory test results have shown that the modulus, and especially the damping behavior, is influenced by the frequency of loading. The D value for sinusoidal waveform is slightly higher than those of the triangle waveform. Furthermore, the D value of rectangle waveform is considerably higher than sinusoidal and triangle waveforms [19].

The Fourier spectra of shear strain time histories of some earthquakes show that the amplitude of the shear strain decays quickly with an increase in frequency [26–30]. Additionally, in-situ soil-specific nonlinear dynamic properties back-calculated from vertical array records during strong ground [31,32] show that modulus and especially damping ratio are dependent on the frequency of loading. Selection of D curve independent of testing loading frequency usually can result in unrealistic amplification of low period components using a ground motion rich in high frequency contents.

Among mechanisms contributing to material damping, it was understood that inertia acting on the individual soil particles and the system as a whole reduce the contact surface between the particles and disturb the stable structure and orientation of grains causing the energy dissipation. In addition, dynamic loading at higher frequency caused an impact between the particles (particle collision) and the tendency of particles to decrease in volume (settlement) resulted in greater interaction between them, causing large energy dissipation [33,34,18,19].

All the cyclic deviator stresses in earlier studies on gravels were applied in uniform sinusoidal cycles at frequencies of up to 0.2 Hz [35]. The low frequency may be selected in order to measure the deformation accurately as well

Table 1: Predominant frequency of some near-fault earthquakes.

Earthquake	Station	Date	Magnitude			Predominant frequency (Hz)			
			M	*Ml*	*Ms*	*L*	*V*	*T*	Average
Kobe, Japan	99999 kJMA	1995/01/16	6.9	–		2.02	3.61	2.01	2.55
Landers	SCE 24 Lucerne	1992/06/28	7.3	–	7.4	9.42	13.01	10.48	10.97
Tabas, Iran	9101 Tabas	1978/09/16	7.4	7.7	7.4	3.84	7.11	4.00	4.98
Bam	Farmandri, 3168/02	2003/12/26	–	–	6.7	4.86	8.38	5.08	6.11
Cape Mendocino	89005 Cape Mendocino	1992/04/25	7.1		7.1	4.74	6.14	4.74	5.21
Chi-Chi, Taiwan	TCU084	1999/09/20	7.6	7.3	7.6	1.94	3.53	1.34	2.27
Kocaeli, Turkey	Sakarya	1999/08/17	7.4	–	7.8	–	8.52	5.85	7.18
Loma Prietas	57007 Corralitos	1989/10/18	6.9	–	7.1	2.76	4.81	2.39	3.32
Northridge	24087 Arleta—Nordhoff Fire Sta	1994/01/17	6.7	6.6	6.7	3.02	8.22	3.48	4.91
Superstitn Hills (B)	286 Superstition Mtn	1987/11/24	6.7	–	6.6	4.41	–	3.91	4.16
Duzce, Turkey	Duzce	1999/11/12	7.1	7.2	7.3	2.16	8.44	1.93	4.17
Erzincan, Turkey	95 Erzincan	1992/03/13	6.9	–	–	1.40	5.55	2.25	3.00
Imperial Valley	942 El Centro Array #6	1979/10/15	6.5	6.6	6.9	3.71	8.98	3.00	5.23
Average						3.69	7.19	3.88	4.93

Note: Closest distances to faults ruptures are less than 10 km. *M*: moment magnitude; *Ml*: Richter local magnitude; *Ms*: surface wave magnitude; *L*: Longitudinal component; *V*: Vertical component *T*: Transversal component.

Table 2: Predominant frequency of some far-field earthquakes.

Earthquake	Station	Date	Magnitude			Predominant frequency (Hz)			
			M	*Ml*	*Ms*	*L*	*V*	*T*	Average
Irpinia, Italy	ENEL/SEA99	1980/11/23	–	6.5	–	2.86	8.46	2.95	4.76
Chi-Chi Taiwan	CHY036	1999/09/20	7.6	7.3	7.6	0.93	5.95	1.82	2.90
Northridge	Saturn St	1994/01/17	6.7	6.6	6.7	3.37	4.40	3.30	3.69
Landers	22074 Yermo Fire Station	1992/06/28	7.3	–	7.4	2.08	7.58	3.16	4.27
Loma Prietas	47524 Hollister—South & Pine	1989/10/18	6.9	–	7.1	1.48	3.90	1.83	2.40
Kocaeli, Turkey	Ambarli	1999/08/17	7.4	–	7.8	1.69	4.47	1.38	2.51
Bam	3170	2003/12/26	–	–	6.7	2.92	5.22	3.39	3.84
Average						2.19	5.71	2.55	3.48

Note: Closest distances to faults ruptures are higher than 20 km; *M*: moment magnitude; *Ml*: Richter local magnitude; *Ms*: surface wave magnitude; *L*: Longitudinal component; *V*: Vertical component *T*: Transversal component.

as equipment limitations. The FFT analysis indicates that predominant frequency of the studied near faults (Table 1) and far fields (Table 2) earthquakes ranges between 1 and 13 Hz. The results of numerical analysis show that the greater part of earthquake energy are in the frequency range of 2–5 Hz [36]. ASTM D3999-91 [37] recommended the frequency variation between 0.5 and 1 Hz for different source of cyclic loads such as those caused by earthquakes, ocean wave, or blast. Moreover, ASTM D3999-91 [37] suggested that cyclic loading equipment used for load or deformation controlled cyclic triaxial tests must be capable of applying a uniform sinusoidal load at a frequency within the range of 0.1–2 Hz.

Based on the results, investigation of E and D in the frequency range of 1 and 5 Hz has especial importance in earthquake engineering.

In the previous dynamic analysis procedure, only the horizontal shear stresses induced by earthquake in the embankment are evaluated and simulated in cyclic triaxial test [38]. However, the results obtained from the finite element analysis and the instrument results raise a question about the reliability of the cyclic tests results conducted at $k_c = \frac{\sigma'_1}{\sigma'_3} = 1$, instead of anisotropic $k_c > 1$ at low confining pressure in soils elements located below sloping surfaces [39]. Young's modulus (at strains less than about 0.001%) of compacted well-graded sandy gravel, consolidated under anisotropic stress-state was evaluated by applying small amplitude cyclic loadings on square prismatic specimens [40]. Moreover, the anisotropy stress condition on G and D parameters in conglomerated rockfill materials was investigated by Aghaei Araei et al. [20].

It seems that there are not many published papers dealing with rate of loading in monotonic tests as well as loading frequency and anisotropy effects on D and especially on E behaviors of the dry and saturated rockfill materials and damping rubber based on element tests. This study looks at these issues via large triaxial tests. Moreover, a series of monotonic and cyclic tests were conducted on metal spring, which does not exhibit any viscous effect (only elastic), for sure, about the accuracy of measurements and to check the equipment capabilities.

2. Triaxial testing system

The large scale triaxial apparatus for conducting tests is equipped with universal electro-hydraulic servo controller for vertical load (actuator). The equipment has the following specifications: Capacity of static load: 500 kN; dynamic load: ±200 kN for bias static load of 300 kN. Frequency ranges between 0.01 and 10 Hz. Waveforms are sinusoidal, triangle and rectangle. Lateral pressure for soil and rock specimen is limited to 2 MPa and 20 MPa, respectively. There are external and internal load cells. The internal load cell with a capacity of 500 kN is submersible with accuracy of 150 N. This combination excludes the effect of piston friction in load measurements. High sensitive non-contact coiled deformation transducers [41] located on opposite sides of the top plate is used to measure the average strain and eliminate the rotational component. The maximum range of measurement is 2.5 mm with the accuracy less than 0.001 mm. The pore pressure sensors are located at the bottom plate with a capacity of 1 MPa and accuracy of 0.4 kPa.

Table 3: Details of large scale triaxial apparatus specification at BHRC laboratory.

Measuring element	Accuracy	Resolution (mV/V)	Carrier frequency (kHz)	Electric transducers, capacity	Amplifiers
Vertical external load cell (large capacity)	150 N	1.5	5	Strain gauge type, 500 kN	EA-410, Calibration: 500, 250 kN, Attenuator: 1, 1/2
Vertical internal load cell (large capacity)	150 N	1.5	5	Strain gauge type, 500 kN	EA-410, Calibration: 500, 250 kN, Attenuator: 1, 1/2
Vertical internal load cell (small capacity)	60	1.5	5	Strain gauge type, 200 kN	EA-410, Calibration: 200, 100 kN, Attenuator: 1, 1/2
Vertical displacement (external LVDT)	0.01 mm	2	5	Strain gauge inductance type,100 mm	EA-410, Calibration: 100, 50 mm, Attenuator: 1, 1/2
Vertical displacement (two sets placed just at top of the specimen and opposite sides)	<0.001 mm	1	20	Twin coil type, 25 mm	EA-330, Calibration:25, 12.5, 5, 2.5 mm, Attenuator: 1, 1/2, 1/5, 1/10
Lateral pressure	0.8 kPa	2	5	Strain gauge flush diaphragm type, 2 MPa	EA-410, Calibration: 2, 1 MPa, Attenuator: 1, 1/2
Pore water pressure	0.4 kPa	2	4.9	Strain gauge flush diaphragm type, 1 MPa	EA-410, Calibration: 1, 0.5 MPa, Attenuator: 1, 1/2
Volume change (internal)	8 cc	10	4.9	Differential pressure type, 4 L	EA-410B, Calibration: 4, 2, 0.8 L, Attenuator: 1, 1/2, 1/5

More details about types of sensors, accuracy and resolution are presented in Table 3.

Data acquisition system has eight independent channels with response frequency of 75 kHz. It can record data for an interval of less than 0.1 ms.

2.1. Accuracy of measurements

The correctness of the results depends on the accuracy of the measurements of both stresses and strains. The obtained results are affected by three sources of errors; compliance, bedding error, and time lag in measurement. The compliance of loading system consists of all parts (top and bottom platens and connections) where the specimen deformation is monitored and determined [42]. In the present study, errors due to apparatus compliance were investigated with reasonable certainty by careful calibration in the laboratory. For this purpose, a metal spring and cylindrical damping rubber specimen were placed into the location normally occupied by specimens where some calibration tests were performed. The results will be discussed in the following section. Also, in this study, deformation properties were obtained by the same test method from very small strain to large strain levels. Therefore, deviation in tests results caused by system compliance was not encountered [24].

On other hand, lower values of stiffness during initial cycles, because of bedding errors, were not observed in hysteresis loop. Bedding error may be high in the case of soft rock, hard soils [43] and gravelly materials [44]. We eliminated bedding effect between specimen cap and specimen by filling the voids between the cap and specimen with the same finer materials. Moreover, bedding error can be reduced through the following method: achieving the final desired height of reconstituted specimens by tapping and rotating the specimen cap on top of the specimen [37]. Therefore, the effect of bedding error can be ignored in these tests with the above mentioned considerations.

Although the data acquisition is simultaneous, possibility of apparent damping at high loading frequency due to time lag in measurement of axial load and axial displacement is also investigated as follows: (1) acquisition of axial displacement after axial load, (2) axial load measured late to axial displacement. No difference in damping ratio was observed in the two methods given above.

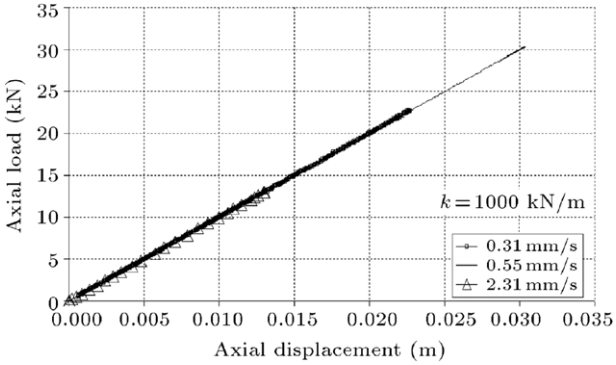

Figure 1: Load–axial displacement results on the elastic spring at different rate of loading.

3. Monotonic and cyclic tests on metal spring and damping rubber

In order to calibrate and check the performance and accuracy of all parts of the triaxial equipment, a series of tests were conducted on spring and damping rubber. The axial load–axial displacement curve for the spring under different strain rates is shown in Figure 1. As illustrated, the speed of loading does not affect the behavior of elastic spring and almost a single straight line is obtained. In other words, when the loading is maximum, at the same time the corresponding displacement is maximum, and there is no time lag. Then, some cyclic tests were performed on the spring under initial static axial load of 13 kN, which induced 13 mm deformation in the spring. The cyclic tests were performed with loading frequency equal to 0.1, 0.2, 0.5, 1, 2, 5 and 10 Hz. The results of spring tested at different loading frequencies under rectangle, sinusoidal and triangle waveforms did not show apparent damping ratio for the linear elastic material (Figure 2). Moreover, the same stiffness was obtained under different waveform and loading frequency, which is equal to 1000 kN/m. Similar results were obtained when initial static axial load was 30 kN. It is worth to note that there is a considerable difference between induced axial displacements under rapid cyclic loading (rectangle waveform) and slow cyclic loading (triangle waveform), as shown in Figure 3. Induced axial displacements decrease as loading frequency increases.

Figure 3 shows the maximum axial displacement ratio for different waveforms on the spring. Induced axial displacement

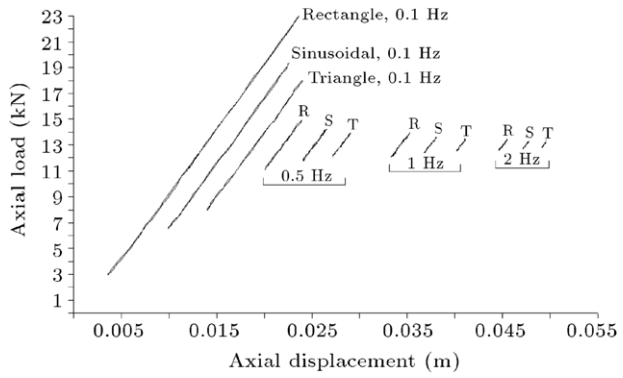

Figure 2: Typical cyclic load–axial displacement result on the elastic spring at different loading frequency (not shifted).

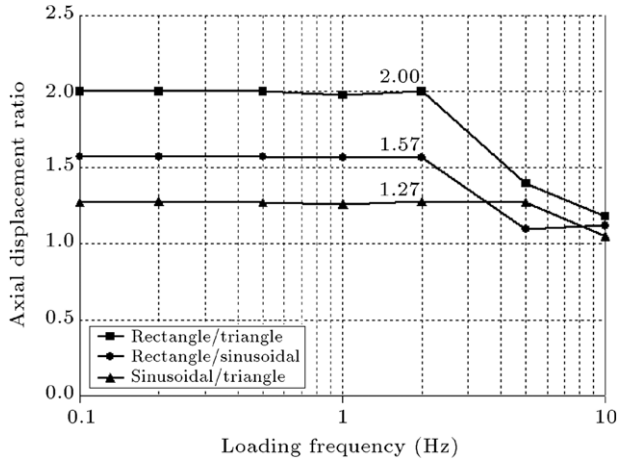

Figure 3: Maximum axial displacement ratio-loading frequency for different waveform in the spring.

by the rapid cyclic loading (rectangle waveform) is two times the triangle waveform ones up to 2 Hz. For better interpretation of the spring behavior, its natural frequency is required. In order to obtain effective mass of the spring for the case of distributed mass system, firstly, the kinetic energy must be calculated. If $\dot{z}$ is equal to the velocity of the top of the spring, the velocity of the spring element with length of l located at a distance y from the fixed end varies linearly with y as follows [45]:

$$\dot{z}_y = \dot{z}\frac{y}{l}. \tag{1}$$

The kinetic energy of the spring can then be integrated to:

$$T = \frac{1}{2}\int_0^l \left(\dot{z}\frac{y}{l}\dot{z}\right)^2 \frac{m_{\text{spring}}}{l}dy = \frac{1}{2}\frac{m_{\text{spring}}}{3}\dot{z}^2. \tag{2}$$

This means the effective mass is to be one third the mass of the spring. Then, the natural frequency of the spring is:

$$f_{n(\text{spring})} = \frac{1}{2\pi}\sqrt{\frac{k_{\text{spring}}}{(1/3)\cdot m_{\text{spring}}}}, \tag{3}$$

with $m_{\text{spring}} = 9.62$ kg and $k_{\text{spring}} = 1000$ kg/cm, $f_{n(\text{spring})}$ is equal to 2.81 Hz. According to Figure 4, at higher frequency ($4f_{n(\text{spring})}$ or >10 Hz), the effect of the waveform on maximum

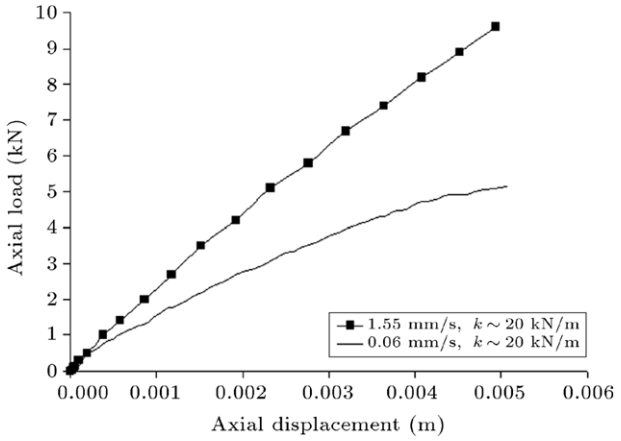

Figure 4: Load–axial displacement results at effective confining pressure of 250 kPa of the damping rubber with diameter of 20 cm and height of 40 cm.

Table 4: Characteristics of cyclic triaxial tests on the damping rubber.

σ_3' (kPa)	$k_c = \sigma_1'/\sigma_3'$	Frequency of loading (Hz)
0	[a]	0.1, 0.5, 1, 5, 10
250	1	0.1, 0.5, 1, 5, 10
250	2	0.1, 0.5, 1, 5, 10

[a] $\sigma_1' = 7.85$ kN.

displacements ratio is negligible. Moreover, in the tested spring under cyclic loading, if the loading frequency is less than $2f_{n(\text{spring})}$, the maximum displacement occurs during cyclic loading (see sinusoidal/triangle waveform curve in Figure 4). The shock response to triangle and rectangle pulse of an undamped spring-mass system for SDOF was studied previously [46].

Moreover, the test results such as load–axial displacement curves on the damping rubber (20 cm diameter, 40 cm height, and unite weight of 12.23 kN/m^3) at effective confining pressure of 250 kPa under speed of 0.06 and 1.55 mm/s are presented in Figure 4. Figure 4 shows a clear non linearity (not linear the stress–strain relation) especially for the smaller loading rate. Stiffness of the damping rubber is about 10 MN/m for rate of 0.06 mm/s and 20 MN/m for rate of 1.55 mm/s. Hence, stiffness increases as rate of loading increases (strain dependent). Moreover, the load and axial displacement versus time results indicates that maximum axial displacement occurs with a time lag for corresponding maximum axial load.

In addition, a series of sinusoidal cyclic loading were conducted on the damping rubber at different conditions (Table 4). For instance, Figure 5 shows axial load–axial displacement loops of the damping rubber at effective confining pressure of 250 kPa and $k_c = 2$ under loading frequency of 0.1, 1 and 5 Hz. The sizes and inclination of the hysteresis loops clearly indicate the effects of the loading frequency on stiffness and damping ratio results.

Cyclic tests results including E–ε_1 and $D - \varepsilon_1$ on the damping rubber at effective confining pressure of 250 kPa and $k_c = 2$ are shown in Figure 6. As shown in Figure 6, E and D decrease with strain level. Moreover, the result indicates that at certain strain, E and D increase as loading frequency increases. Variation of D with loading frequency is less pronounced, and its value at frequency of 5 and 10 Hz does not show considerable difference. Variation of damping ratio for frequency of 0.1 and 10 Hz ranges between 15% to maximum 25%. The $E-\varepsilon_1$ values at

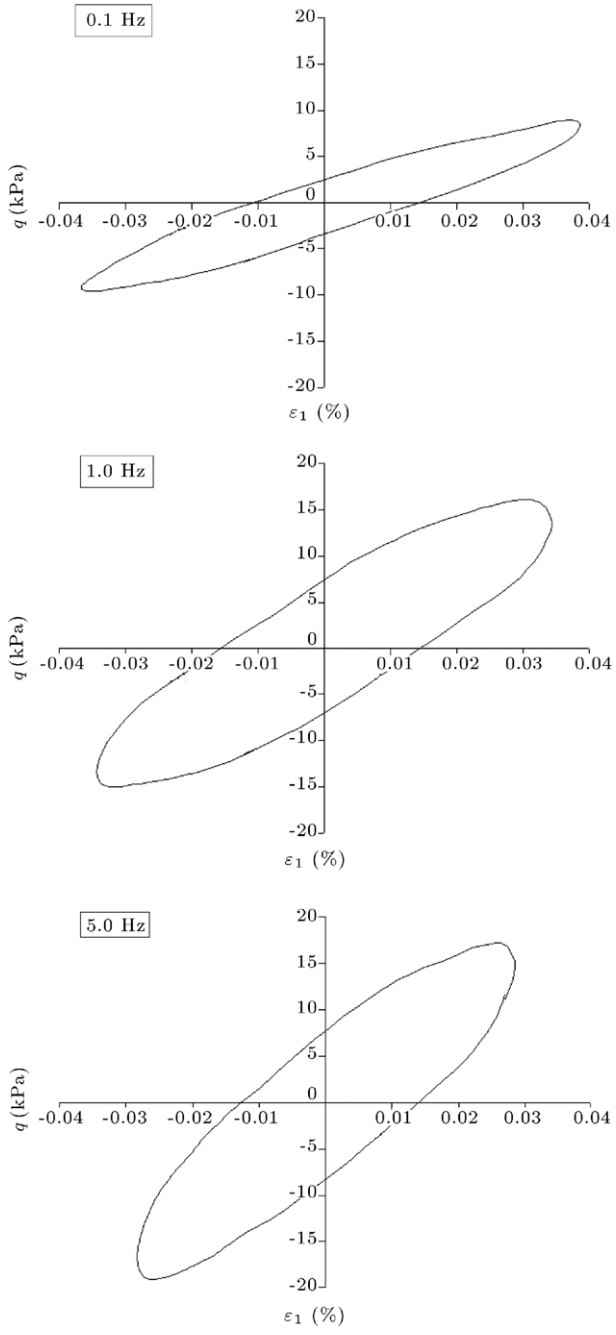

Figure 5: Example of cyclic load–axial displacement results on the damping rubber at effective confining pressure of 250 kPa and $\sigma'_1/\sigma'_3 = 2$ under different loading frequency.

unconfined anisotropic ($k_c = 2$) condition is slightly higher than the value of the isotropic condition at effective confining pressure of 250 kPa, but less than the value of the anisotropic ($k_c = 2$) condition at effective confining pressure of 250 kPa [47]. Moreover, damping ratio at anisotropic ($k_c = 2$) unconfined condition is similar to isotropic condition at effective confining pressure of 250 kPa, but less than anisotropic ($k_c = 2$) condition at effective confining pressure of 250 kPa [47]. Accurately speaking, in damping rubber for a given strain level, E increases with k_c and confining stress while D is rather insensitive to the confining stress which increases with k_c.

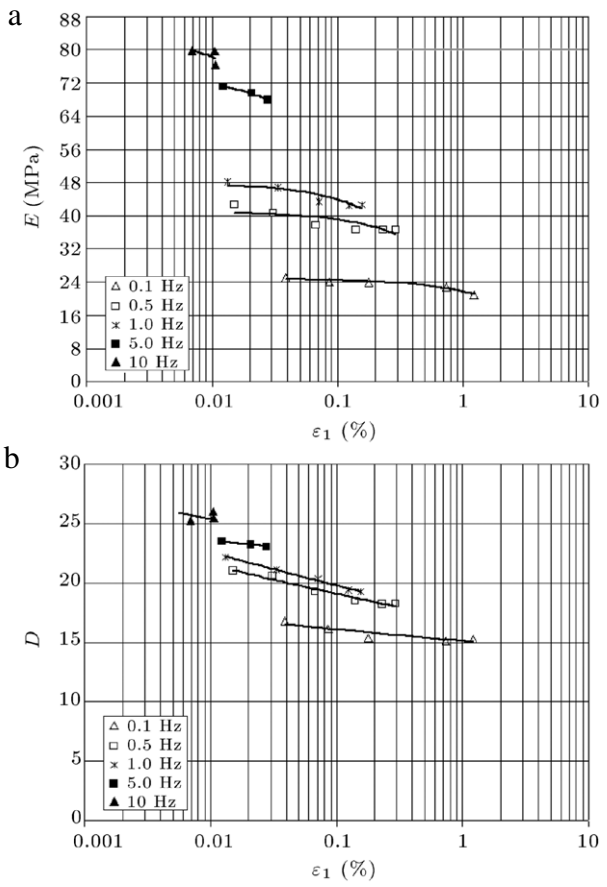

Figure 6: Cyclic tests results of the damping rubber at effective confining pressure of 250 kPa and $\sigma'_1/\sigma'_3 = 2$. (a) E versus axial strain; and (b) D versus axial strain.

4. Rockfill test specimens

4.1. Material properties

In this study, the tested gravelly rockfill sample was obtained from the shell material of the under-construction Lower Siah-Bisheh Concrete Faced Rockfill Dams (CFRDs) in Iran [18]. Table 5 summarizes the main characteristics of the material, including rockfill name, size distribution, Point Load Strength index, Loss Angeles abrasion, dry density, optimum water content and specific gravity. The quarry blasting produces the S.SBLIV material from quarry No. IV, which was used for the Lower Siah-Bisheh CFRD. The individual particle is composed of Lime rock. The gradation curve of the material for triaxial testing was obtained with maximum particle sizes of 50 mm (1/6 diameter of large scale triaxial specimen, which is 30 cm), Figure 7. The material consist of 3.8% fine grains (<0.075 mm).

Maximum dry density was estimated for the sample according to Modified Proctor [48] and modified for oversize (20% higher than 19 mm) percentage [49]. Specific gravity (Gs) is 2.62 and minimum void ratio (e_o) is 0.174.

4.2. Specimen preparation

Tests were conducted on large scale specimens with the dimensions of 30 cm diameter and 60 cm height, using the large scale triaxial equipment at the BHRC, Iran. Specimens were

Table 5: Characteristics of gravelly material used in large scale triaxial testing.

Material symbol		S.SBLIV
Maximum particle size (mm)		50
$D_{(10)}$, $D_{(30)}$, $D_{(50)}$, $D_{(85)}$ (mm)		0.5, 2.5, 6.5, 25
Passing #200 (%)		3.8
Is (ASTM D5731)	Submerged for 7 days	2.89
	Natural water content	2.82
Loss angeles abrasion for no. of rotations of 1000 (%) (ASTM C131)		44.9
$\gamma_{d(\max)}$ (kN/m^3)	ASTM D1557 (C-method)	21.8
w_{opt} (%)		6.1
G_s (bulk specific gravity—oven dry) (ASTM C127)		2.62
e_0		0.174

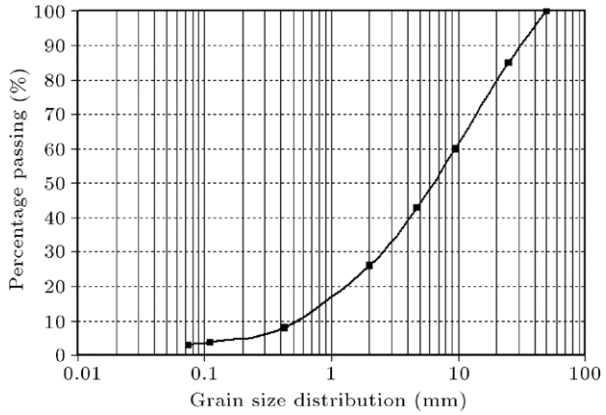

Figure 7: Grain size distribution for modeled rockfill materials in triaxial testing.

compacted to required dry density in a split mold using a vibrator compactor operating at a frequency of 60 cycles. A silicone type membrane with a thickness of 2.5 mm complying with ASTM D3999 [37] and ASTM D4767 [50] was used to encase the specimen and provide reliable protection against leakage. The Young's modulus (E_m) of the used membrane is 750 kPa. The increase of deviator stress for $\varepsilon_1 = 15\%$ (0.15 in decimal form) is less than 4 kPa. We ignore membrane correction effect over the measured deviator stress. The interaction between the specimen, membrane, and confining fluid has an influence on monotonic and cyclic behaviors. Changes in pore water pressure can cause changes in membrane penetration in specimens of cohesion-less soils [51]. We eliminated membrane penetration effects by putting the finer soil in the surface of specimens to create a smooth surface.

Specimens were reconstituted in six layers. For each layer, the necessary quantity by weight of each granulometric class was weighed and mixed with the appropriate water content. In the saturated specimen, after passing the CO_2 and applying a vacuum for a period of 24 h, the sample was partially saturated by allowing de-air water to pass through the base of the triaxial cell and removing air bubbles. To achieve full saturation (Skempton B-value greater than 95%), back-pressurization was used.

5. Monotonic loading triaxial tests

Monotonic triaxial compression tests were used to study the stress–strain–strength behavior of the rockfill materials. Eight monotonic Consolidated Drained (CD) triaxial tests were performed at dry densities of 21 and 21.5 kN/m^3 and different confining pressures on the saturated specimens (Table 6). All monotonic tests were performed with the use of strain-controlled compression loading system. After applying the predefined confining pressure, the axial load was applied to axial strain up to about 15%. The imposed axial strain rate was 0.5 mm/min. During the test, the amount of axial stress, axial strain and volumetric strain were recorded. Also, one more dried specimen with dry density of 21.5 kN/m^3 was sheared under a strain rate of 300 mm/min.

5.1. Presentation of the results

Table 6 presents the summary of the results of the monotonic triaxial tests. Maximum friction angles are calculated for each single confining pressure, assuming $c = 0$ and using the following equation:

$$\sin\phi' = \left(\frac{\sigma_1' - \sigma_3'}{\sigma_1' + \sigma_3'}\right)_{\max}. \quad (4)$$

Generally, ϕ' for the materials decreases with an increase in the confining pressures; the internal friction angle for under study materials ranges between 46° and 38° for the confining pressures ranging from 200 to 1500 kPa (Table 6). Figure 8 shows the value of deviator stress and volumetric strain versus axial strain for different materials at different dry densities. Generally, the higher the value of dry density, the more the amount of deviator stress is. As it is expected, axial strain at failure increases with an increase in confining pressure. The dilation in volumetric strain decreases considerably with any increase in confining pressure. According to the results obtained, there is no remarkable difference between the studied materials with respect to internal friction angles at two dry densities.

Figure 9(a) shows deviator stress and axial strain versus time of the dry specimen under confining pressure of 200 kN/m^3 and strain rate of 300 mm/min. As shown in Figure 9(a), at the initial stage of loading, when the deviator stress is maximum (around 7 s), the corresponding axial strain is not maximum (time lag existed). So, it seems that in the rockfill materials at high speed of loading, rate dependent behavior can be observed. Figure 9(b) shows deviator stress versus axial strain. Comparing to saturated condition, one may say that the maximum deviator stress of the dry specimen is 1.5 times higher than saturated ones. Some part of difference may be attributed to high speed of loading of the dry specimen.

6. Cyclic testing programs

6.1. Testing procedure

24 cyclic triaxial tests were carried out in this research according to ASTM D3999 [37] (Table 7). The specimens were first subjected to the required consolidation pressures with respect to the stress levels in typical high rockfill dams or CFRDs. Then, specimens were loaded under initial isotropic condition ($k_c = \sigma_1'/\sigma_3' = 1$) and anisotropic condition ($k_c = 2$). During the tests the amount of anisotropy coefficient was fixed by applying the desired loads from the load cell of triaxial equipment. Staged tests were performed to save cost and time. Forty cycles sinusoidal loading, with the desired loading frequencies,

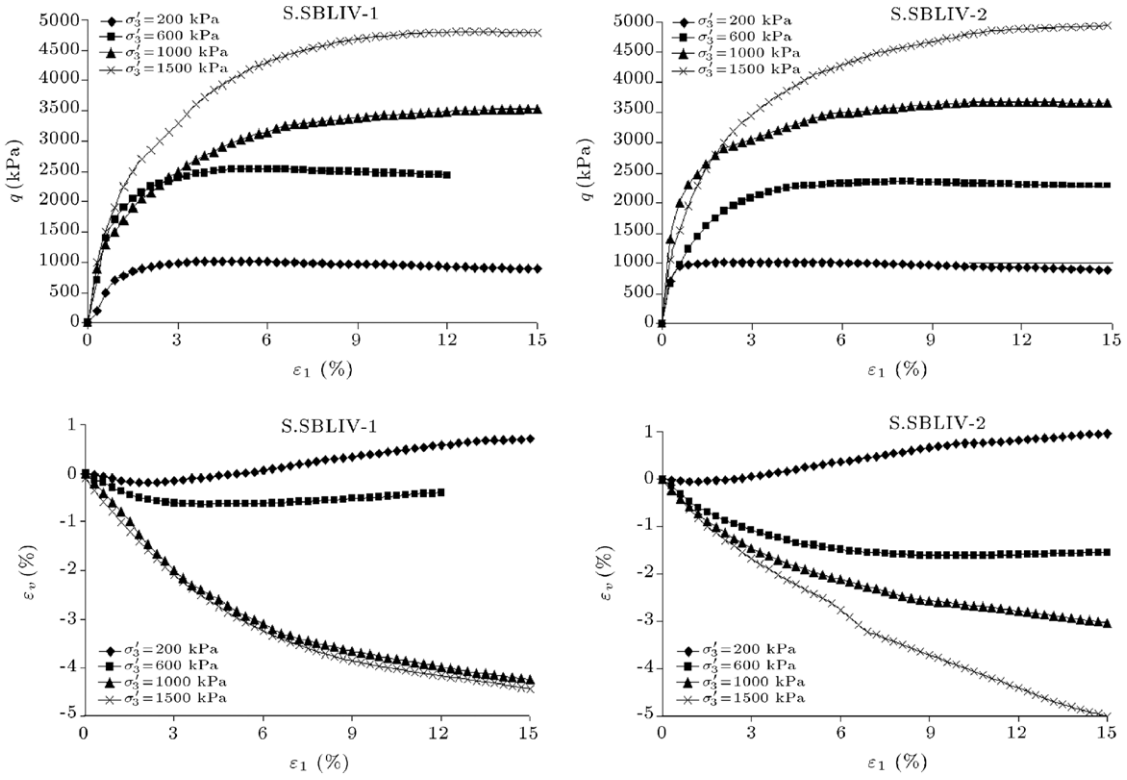

Figure 8: Deviator stress–volumetric strain versus axial strain curves.

Table 6: Summarized information and results of large scale monotonic triaxial tests.

Rockfill type	γ_d (kN/m^3)	Dr (%)	σ_3' (kPa)	Volume change at end of isotropic consolidation (L)	q_{max}/σ_3'	$\varepsilon_v(q_{max})$ (%)	ϕ'° (Peak)	B_g (%) for particle size ranges from		
								0.075–50 mm	0.075–4.75 mm	4.75–50 mm
			–	–	–	–	–	5.4	2	3.6
			200	0.397	5.05	0.078	46	6.3	3.3	2.9
S.SBLIV-1	21.0	96	600	0.623	4.23	0.64	42.9	7.1	2.7	4.4
			1000	0.873	3.54	4.4	39.45	8.4	3.4	5
			1500	0.904	3.2	4.4	37.9	9.1	5.3	3.9
			–	–	–	–	–	6	1.5	4.5
			200	0.396	5.1	−0.027	46.2	6.3	4.5	5.9
S.SBLIV-2	21.5	98	600	0.519	3.93	1.55	41.6	8.6	4.7	5.2
			1000	0.593	3.66	2.68	40.2	10.6	4.1	6.5
			1500	0.658	3.29	4.84	38.25	10.1	3.5	6.9

Table 7: Characteristics of testing program according to ASTM D3999 under sinusoidal waveform.

Material symbol/specimen condition	σ_3' (kPa)	$k_c = \sigma_1'/\sigma_3'$	Number of cycles	Frequency of loading (Hz)	Total no.
S.SBLIV/saturated	100, 200, 400, 600, 1000, 1500	1	40	1, 5	12
S.SBLIV/saturated	200, 400	2	40	1, 5	4
S.SBLIV/dry	200, 400	1	40	1, 5	4
S.SBLIV/dry	200, 400	2	40	1, 5	4

were applied at a very small strain level [37]. This number of cycles corresponds to a loading induced by an earthquake with a magnitude of 7.5 on the Richter scale [52]. Test results for cycles 1–40 have been recorded. The excess pore pressure that had developed during this cyclic loading was dissipated by opening the drainage valve, so that the original effective stresses could be regained in the saturated specimens. This procedure was then repeated at higher strain levels (about twice the initial amplitude) until the maximum strain level was achieved. Axial loads, vertical displacements, volume changes and pore pressures were measured at periodic intervals of 0.020 and 0.004 s, respectively, for the applied sinusoidal waveform with frequencies 1 and 5 Hz. Thus, the sampling frequency was 50 data points per cycle (according to ASTM D3999 [37] minimum sampling rate should be 40 data points per cycle). Cyclic tests were performed under stress-control.

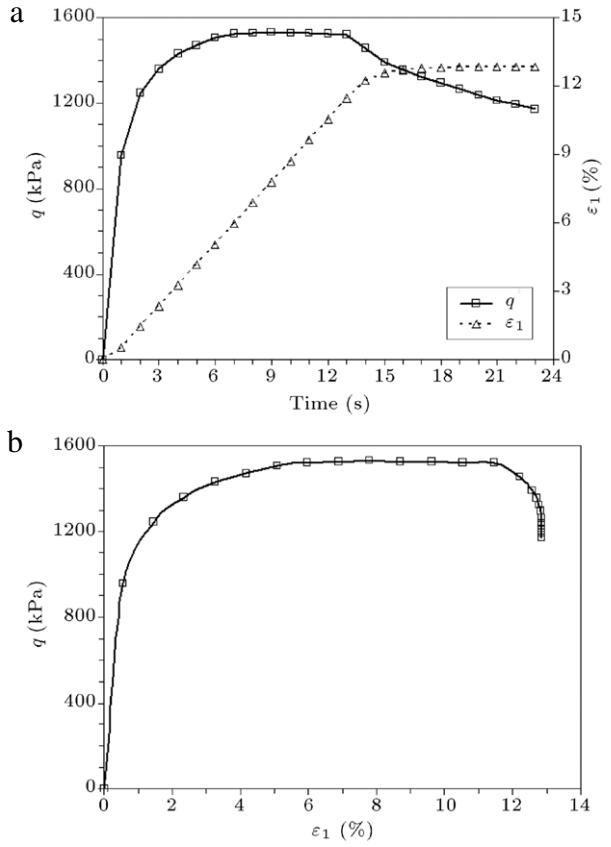

Figure 9: Test results of the dry S.SBLIV specimen at confining pressure of 200 kPa and strain rate of 300 mm/min. (a) Deviator stress–axial strain versus time; and (b) deviator stress–axial strain.

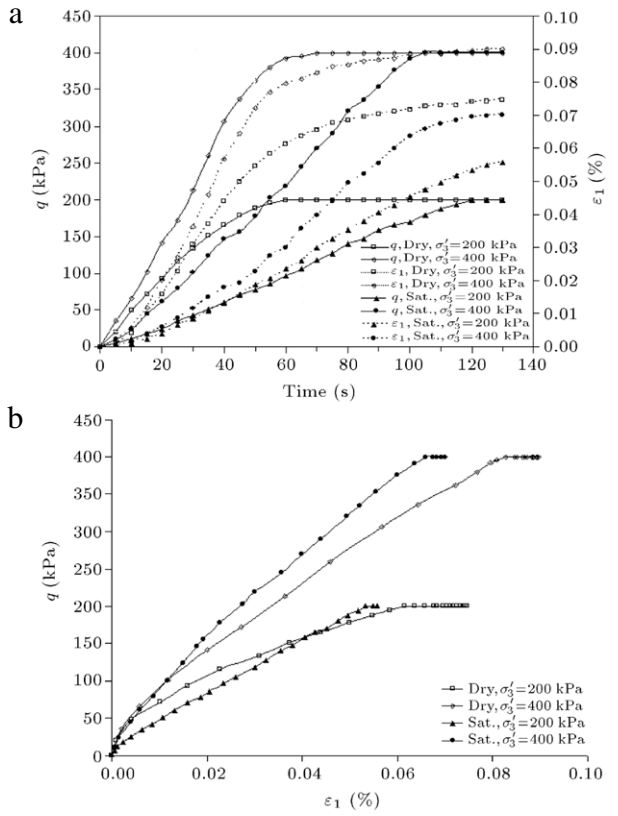

Figure 10: Test results of the dry and saturated S.SBLIV specimen at confining pressure of 200 and 400 kPa. (a) Deviator stress–axial strain versus time; and (b) deviator stress versus axial strain.

6.2. Monotonic triaxial tests for creation of anisotropic condition

The initial phase of static shear stress application is envisaged as representing a sustained static pre-earthquake state of stress which exists in a soil element beneath sloping surfaces. Based on the above monotonic tests and instrument data results in the rockfill dam in which horizontal stress ratio (P_h/P_v) ranges between 0.1 and 1.0 with an average of 0.55 [39], $k_c = 2$ was selected in this study only for low confining pressures.

Dry and saturated specimens with dry density of 21.5 kN/m^3 at confining pressure of 200 and 400 kPa were loaded till anisotropic conditions were achived ($k_c = 2$). Tests results including deviator stress–axial strain versus time and deviator stress versus axial strain are presented in Figure 10. Time required to obtain maximum axial load of the saturated specimen is nearly 2 times the dry specimen. The initial modulus of dry specimen is higher than saturated samples (Figure 10). The result indicates that secant modulus increases as confining pressure increases.

6.3. Cyclic test results

Tests results, including the Young's modulus and damping ratio versus axial strains, have been calculated based on the stress–strain hysteresis loop for the 1–40th cycles according to ASTM D3999 [37].

6.3.1. Young's modulus

The E versus γ data points at 10th cycle under confining pressure of 100, 600, 1000 and 1500 kPa are shown in Figure 11.

In this study, for comparison proposes, it was considered that the most appropriate E value was at the 10th cycle, since this is considered to be an average representation for the earthquake in this dam region. It can be seen that E is strongly dependent on the axial strain. At low strain amplitudes, the modulus is nearly constant and at its highest value, E_{max}, but it decreases while the strain amplitude is increasing. As it is expected, as confining pressure increases, the E versus ε_1 values increase. However, for studied rockfill materials, as confining pressure increases, its effect on the values of E decreases; the rate of increase in E at low confining pressure is higher than the corresponding value at a higher confining pressure. It is observed that, in general, the E values increase as loading frequency increases, especially at the axial strains less than 0.01% (Figure 11). However, for these materials, as axial strain increases, loading frequency effect on the values of E decreases; the rate of increase in E at low strains is higher than the corresponding value at higher strain.

Generally, in this discrete rockfill materials, increase in frequency increases the magnitude of acceleration in vertical direction at the upper part of the large triaxial specimen. Higher acceleration on the particles of soil reduces the modulus due to inertia effect [33]. The absolute effect of inertia is to reduce the modulus considerably, while the reduction in modulus may be compensated by the frequency effect. The net effect is to slight increase the modulus.

6.3.2. Damping ratio

Figure 12, for instance, shows stress–strain hysteresis loop at almost the same amplitude of deviator stress and strain for

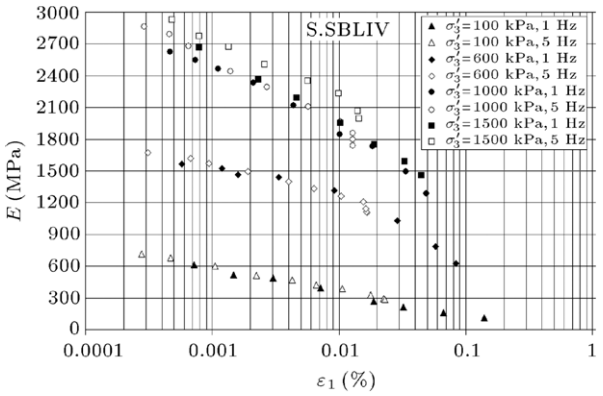

Figure 11: Variations of Young's modulus versus axial strain of saturated isotropic specimen at confining pressures 100, 600, 1000 and 1500 kPa under loading frequency of 1 and 5 Hz.

S.SBLIV material at effective confining pressure of 400 kPa at the 10th cycle under loading frequency of 1 and 5 Hz. There are some differences in the hysteresis loop. The obtained hysteresis loop indicates the importance of loading frequency on damping results.

Figure 13 presents the D versus ε_1 data points at 10th cycle for materials tested at confining pressures of 100, 600, 1000 and 1500 kPa under loading frequencies of 1 and 5 Hz with those of Seed et al. [8] and Rollins et al. [35]. The damping ratio decreases as confining pressure increases.

It is worth mentioning here that by increasing the loading frequency, damping ratio increases, not only at low strain but also at medium and higher strain levels. For tests at loading frequency of 1 Hz, at high strain, data lie completely within the main curve proposed previously; whereas at low strain (axial strain less than 0.005%), considerable portion of the data lie above upper bound proposed by Seed et al. [8]. However, at higher loading frequency (5 Hz) the damping ratios completely fall above the upper bound trend observed by Seed et al. [8].

The high values of damping at loading frequency of 5 Hz for the rockfill materials with low void ratio may be attributed to sensitivity of their structure to loading frequency, due to increased collision of soil particles resulting in high dissipation of energy at contact points of the particles and more settlement [18,33]. Generally, in this discrete rockfill material, at higher frequency, almost all particles try to move, where damping ratio increases by the inertia effect.

For controlling above statement, the resonant frequency of the triaxial specimen must be calculated. The case of the distributed mass rockfill specimen in triaxial equipment under cyclic loading can be approximated to a spring and dashpot, subjected to a sinusoidal varying force ($F_0 \sin(2\pi ft)$), where f = frequency of loading, and F_0 is the maximum amplitude of loading. The differential equation of motion for this system can be given by:

$$(m_{\text{eff}})\ddot{z} + (k_{\text{soil}})\dot{z} + (c_{\text{soil}})z = F_0 \sin(2\pi ft), \tag{5}$$

where m_{eff} is equal to mass of cap ($m_{\text{cap}} = 14.48$ kg) as well as effective mass of the specimen (at strain less than 0.1%, it may be assumed that the velocity of soil particle varies linearly with length of specimen, and rockfill specimen is similar to the case of spring), k_{soil} is the soil stiffness, which changes by the loading frequency and strain, and c_{soil} is the viscous damping of soil. For the steady-state motion, f_{ms}, the frequency at maximum amplitude (the resonant frequency) of the soil specimen is:

$$\begin{aligned} f_{\text{ms}} &= f_{\text{ns}}\sqrt{1-2D^2} \\ &= \frac{1}{2\pi}\sqrt{\frac{k_{\text{soil}}}{m_{\text{cap}} + (1/3)\cdot m_{\text{soil}}}}\cdot\sqrt{1-2D^2}, \end{aligned} \tag{6}$$

where damping ratio is $D = \frac{c_{\text{soil}}}{c_{c(\text{soil})}} = \frac{c_{\text{soil}}}{2\sqrt{k_{\text{soil}}\cdot m_{\text{eff}}}}$, and $c_{c(\text{soil})}$ is the critical damping. Then the high strain and low strain natural frequencies of the rockfill specimen at confining pressure of 100 kPa are ranges between 3 and 7 Hz. The corresponding values at confining pressure of 1500 kPa are ranges between 10 and 14 Hz. Therefore, coinciding natural frequency of the specimen and cyclic loading frequency at 5 Hz especially at low confining pressure may happen.

Generally, the frequency effect on damping ratio is more remarkable than on modulus. This may be attributed to the effects of frequency and inertia among many other reasons. In the discrete rockfill materials, the effect of frequency is to increase both modulus and damping, while the effect of inertia is to reduce the modulus but increase damping.

6.3.3. Effects of loading waveforms on induced maximum axial displacement ratio

Similar to the case of spring, the effects of waveforms on induced maximum axial displacement ratio are investigated on S.SBLIV specimen. The specimens are loaded under triangle, sinusoidal and rectangle waveforms, and the loading frequency

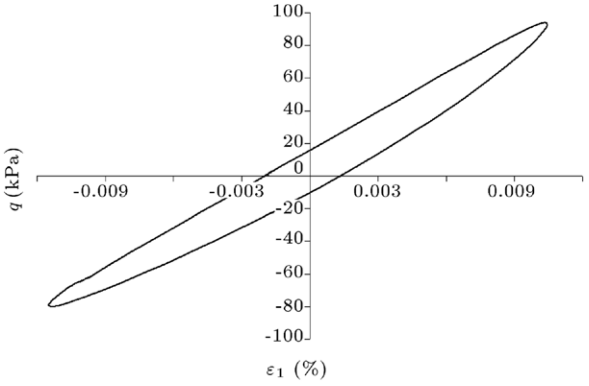

(a) 1 Hz.

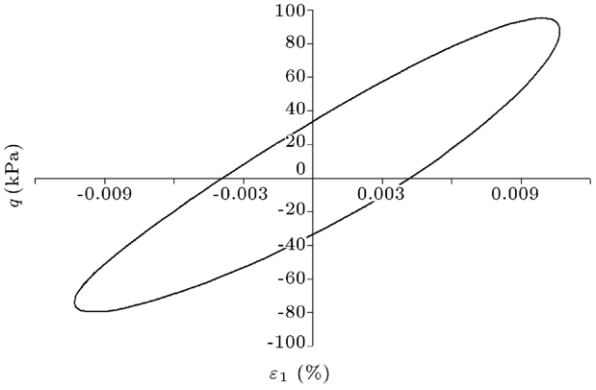

(b) 5 Hz.

Figure 12: Stress–strain hysteresis loop at the 10th cycle for S.SBLIV material at effective confining pressure of 400 kPa and under loading frequencies.

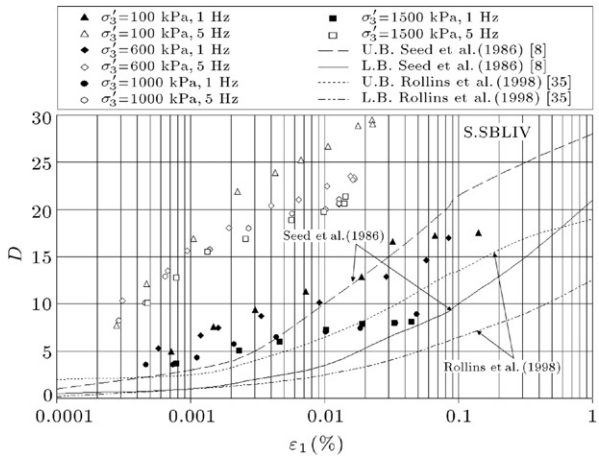

Figure 13: Damping ratio versus ε_1 relationships of the saturated isotropic specimen at different confining pressures and loading frequency.

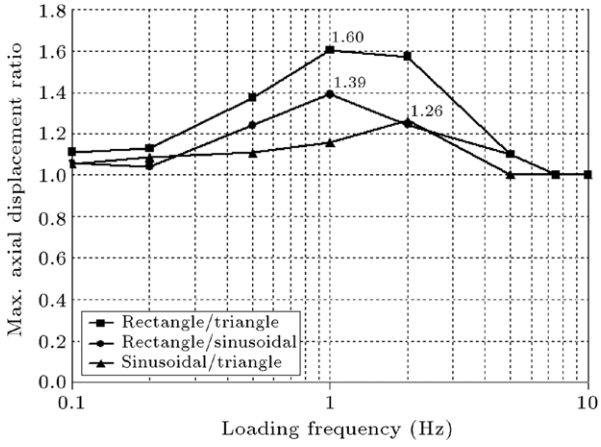

Figure 14: Maximum axial displacement ratio-loading frequency for different waveform of the saturated isotropic S.SBLIV specimen at confining pressure 1000 kPa.

ranges from 0.1 to 10 Hz. Maximum axial displacement ratio versus loading frequency for different waveform of the saturated isotropic S.SBLIV specimen at confining pressure 1000 kPa are shown in Figure 14. Comparing Figures 3 and 14 indicate that there are two main differences:

(a) The maximum axial displacement ratio is lower for rockfill, and
(b) Not constant with loading frequency, reaching the maximum for frequencies between 1 and 2 Hz.

6.3.4. *Effect of k_c for dry and saturated specimens*

Figures 15 and 16 show the variations of the E–ε_1 of the dry and saturated specimens under following conditions: loading frequency = 1 and 5 Hz, confining pressures = 200 kPa and 400 kPa, isotropic ($k_c = 1$) and anisotropic initial stress ($k_c = 2$).

The Young's modulus of the dry specimen is higher than of the saturated ones. The results indicates that E values at axial strain less than 0.005% increase as loading frequency increases. It can be seen that in the anisotropic condition, higher amount of Young's modulus is obtained (Figures 15 and 16). This is because of higher amount of initial $\sigma_m' = (\sigma_1' + 2\sigma_3')/3$ at anisotropy state. Generally, compared to frequency, saturation and confining pressure, the effect of k_c on increasing E is clear.

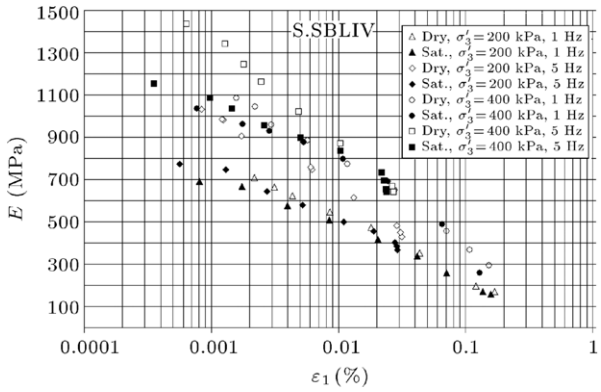

Figure 15: Results of E–ε_1 for dry and saturated isotropic specimens at confining pressures of 200 and 400 kPa and loading frequency of 1 and 5 Hz.

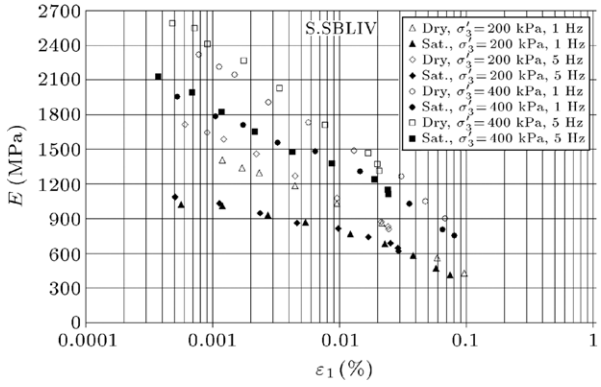

Figure 16: Results of E–ε_1 for dry and saturated anisotropic specimens at confining pressures of 200 and 400 kPa and loading frequency of 1 and 5 Hz.

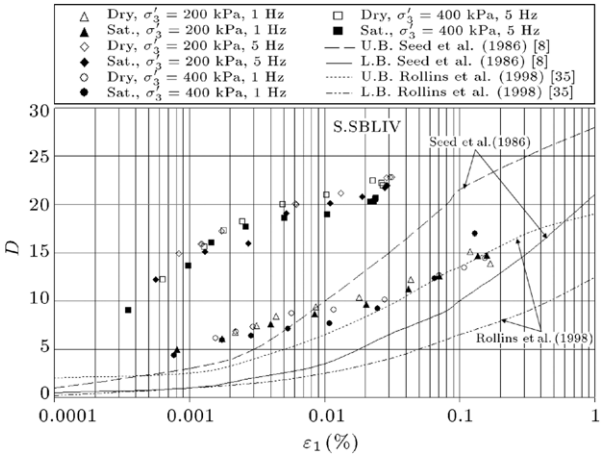

Figure 17: Results of D–ε_1 for dry and saturated isotropic specimens at confining pressures of 200 and 400 kPa and loading frequency of 1 and 5 Hz.

Figures 17 and 18 indicate that the damping ratio in dry specimen is higher than of the saturation specimen. The figures clearly show that D versus ε_1, at certain strain, increases as loading frequency increases. Moreover, at certain strain, the D values for the isotropic condition are slightly higher than of the anisotropic condition. Generally, the main influence is that of the loading frequency.

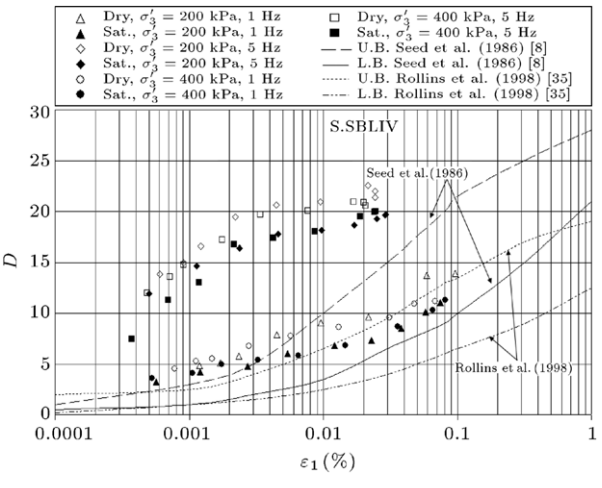

Figure 18: Results of D–ε_1 for dry and saturated anisotropic specimens at confining pressures of 200 and 400 kPa and loading frequency of 1 and 5 Hz.

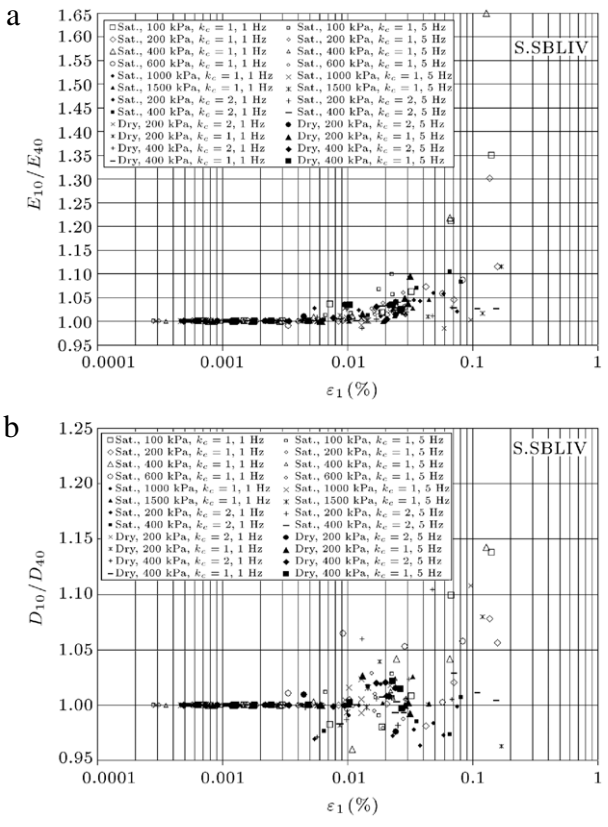

Figure 19: Effect of number of cycles on (a) E_{10}/E_{40}, and (b) D_{10}/D_{40} results versus axial strains of the dry and saturated isotropic and anisotropic specimens.

6.3.5. Variation of E and D with number of cycles

Figure 19(a), for instance, shows the test results of the dry and saturated isotropic and anisotropic specimens including the effects of the number of cycles on E value (i.e. E_{10}/E_{40}; E_{40} = modulus E for 40th cycle) versus axial strain. Generally, the values of E_{10}/E_{40} increase at strain between 0.005% and 0.1%. The values of E_{10}/E_{40} are less than 1.2 at strain less than 0.05%. The values of E_{10}/E_{40} increase markedly at axial strain higher than 0.05%. A larger increase seems casual. The E_{10}/E_{40} ratios for

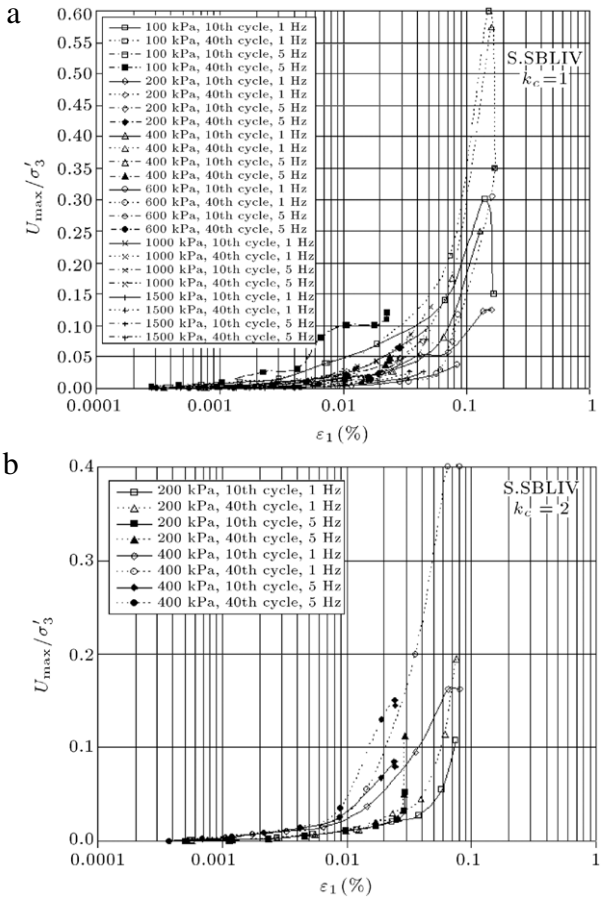

Figure 20: Variations of excess pore water pressure ratio at 10th and 40th cycles versus axial strain of the saturated specimen. (a) Isotropic, and (b) anisotropic.

anisotropic condition have the lowest variation in comparison to tested specimens in isotropic condition.

Variations of D_{10}/D_{40} (D_{10} = damping D for 10th cycle) versus axial strain of the dry and saturated isotropic and anisotropic specimens are shown in Figure 19(b). Results indicate that the effects of the number of cycles over damping ratio are slightly complicated, and it is not possible to draw any definitive conclusion. However, the variations of D_{10}/D_{40} range from 0.95 to 1.15 for strain up to 0.1%. It seems that the D_{10}/D_{40} results were not significantly affected by the number of cycles up to strain less than 0.005% for the rockfill materials, but beyond the mentioned strain, the results were strongly affected. The D_{10}/D_{40} ratio of the dry anisotropic specimen under frequency of 1 Hz have the higher variation in comparison to dry isotropic specimen.

6.3.6. Variation of excess pore water pressure ratio

Figure 20 shows the variations of excess pore water pressure ratio at 10th and 40th cycles versus axial strain under loading frequencies of 1 and 5 Hz. The excess pore water pressure ratio of the isotropic and anisotropic specimens at low confining under loading frequency of 5 Hz is slightly higher than of 1 Hz. The results show that the excess pore water pressure ratios are less dependent on loading frequency and more dependent on imposed strain level.

Since the frequency effect was observed in the strain levels lower than 0.005%, and there is no meaningful build up of pore

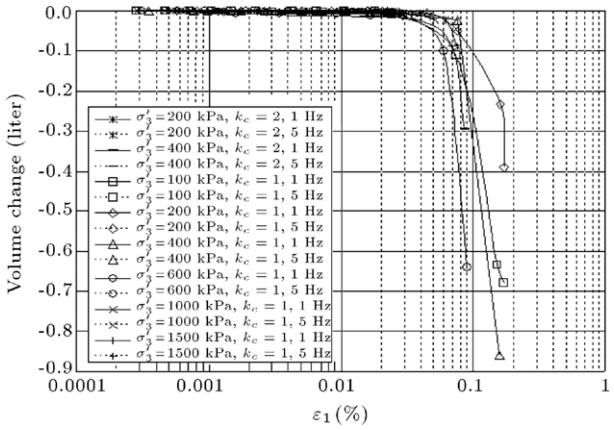

Figure 21: Results of volume change versus axial strain at different loading frequency and confining pressures of the isotropic and anisotropic saturated specimens.

water pressure at this strain level, therefore, any effect of pore water pressure on the frequency effect is negligible.

6.3.7. Variation of volume change and permanent axial displacement

In stage loading, when the pore pressure was released by opening the drainage valve, the volume of the specimen decreases and thus the specimen becomes a little denser. The change in volume is dependent on the axial strain amplitude, the number of strain cycles applied, confining pressure, and the specimen type. Test results of the high compacted rockfill indicates that maximum volume change due to drainage of the specimen at axial strains 0.005% and 0.05% is 0.013 and 0.7 L, respectively (Figure 21). Volume change in percent at axial strain of 0.05% is less than 1.5%. Moreover, the change in density due to drainage is less than 1% for axial strain of 0.1%. The change in volume of the saturated anisotropic specimens is slightly lower than of the isotropic specimen.

According to ASTM D3999 [37] and ASTM D4015 [53], a soil material typically behaves like an elastic solid exhibiting a non-destructive response to the application of cyclic loading below a threshold axial strain level of $<0.01\%$, and many measurements may be made on the same specimen and with various states of ambient stress. It is therefore believed that the re-use of samples for higher strain amplitudes (i.e. up to 0.1%) still gives reasonably good results if the number of strain cycles applied is limited [8].

Figure 22(a) and (b) show the permanent axial deformation versus axial strain of the saturated isotropic and anisotropic specimens in cyclic tests, respectively. Permanent axial deformation at the axial strain less than 0.01% is negligible (less than 0.2 mm) and the height of the specimen decreases. Generally, high compacted specimen under low frequency (1 Hz) cyclic loading at low confining pressure, undergo increase in height at axial strain higher than 0.05%, but at high confining pressure and high loading frequency (5 Hz), the height of specimen decreases continuously. Maximum permanent axial deformations at the axial strain of 0.05% are less 0.5 mm and 1 mm of the isotropic and anisotropic specimens, respectively. Figure 22(c) shows the permanent axial deformation versus axial strain of the dry isotropic and anisotropic specimens in cyclic tests. At certain strain, the anisotropic dry specimen under low confining pressure experiences higher permanent axial deformations compared to isotropic condition. It is worth to note that the permanent axial deformation increases as loading frequency increases.

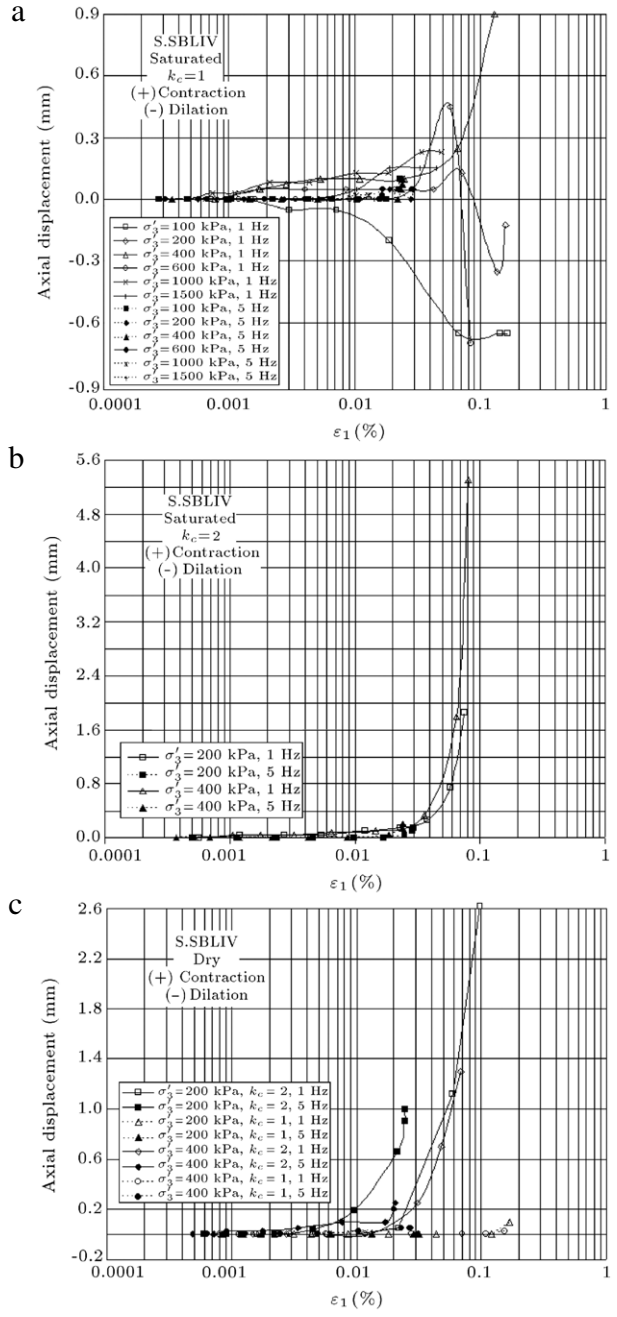

Figure 22: Variations of permanent axial displacement versus axial strain at different loading frequency and confining pressures. (a) Saturated isotropic; (b) saturated anisotropic; and (c) dry isotropic and anisotropic specimens.

6.3.8. Effect of particle breakage

Breakage of the particles was observed during the triaxial tests. The breakage is usually expressed quantitatively by the Breakage Index, B_g [54,55]. The value of B_g is calculated by sieving the sample using a set of sieves before and after testing. The percentage of particles retained in each sieve is determined at both stages. Due to breakage of particles, the percentage of the particles retained in large size sieves will decrease and the percentage of particles retained in small size sieves will increase. The sum of the decreases will be equal to the sum of increases in the percentage retained. The decrease (or increase) is the value of the breakage factor, B_g.

Table 8: Marsal breakage index at the end of cyclic loading of the S.SBLIV specimen.

Specimen condition	σ_3'(kPa)	$k_c = \sigma_1'/\sigma_3'$	For particle size ranges B_g (%) from		
			0.075–50 mm	0.075–4.75 mm	4.75–50 mm
Saturated	100	1	6.8	1.8	6.8
	200	1	6.8	2.2	6.1
	400	1	6.2	1.9	5.7
	600	1	6.5	3	6.5
	1000	1	6.3	2.7	5.1
	1500	1	6.1	1.9	4.9
Dry	200	1	6.8	2.6	4.5

B_g values after construction and monotonic tests of the different particle sizes are presented in Table 6. The results indicates that B_g increases as confining pressure increases (B_g = 10.1% at $\sigma_3' = 1500$ kPa). Considerable amount of B_g is related to breakage of particle at the specimen construction stage. The average value of B_g is 8.3%.

Studies show that particles more susceptible to breakage materials have higher damping ratio [56–58]. The values of B_g at the end of cyclic tests are presented in Table 8. In comparison to monotonic tests (B_g = 8.3%), the average value of B_g in cyclic loading (6.5%) decreases. It seems that B_g does not have considerable value in cyclic test and is strongly dependent on strain level applied. Generally, as confining pressure increases, B_g for gravel and sand portions of rockfill materials decreases slightly in cyclic tests. This may be due to less strain application on specimens and reduction of stress concentration at particle contacts. There is no considerable difference between Point Load Index in dry and saturated particle. So, same B_g values in dry and saturated specimens may be expected (Table 8).

7. Summary and conclusions

Monotonic and cyclic tests were carried out on triaxial specimens of a damping rubber and a modeled rockfill materials. Based on the literature and previous laboratory test results, assessment of loading rate and anisotropy over the damping rubber and rockfill behaviors by triaxial test is suitable. The calibration tests on the elastic spring were conducted in order to ensure the accuracy of the measurements. Based on the studies described in the text, it may be concluded that:

- The response to the loading frequency in elastic metal spring is completely different from those of the damping rubber and rockfill materials. Spring does not exhibit any viscous properties (only elastic), but damping rubber exhibits both nonlinear (strain dependent) and viscous effects.
- Generally, increasing strain level causes increase of damping and decrease in Young's modulus in the rockfill materials, but in damping rubber, increasing strain level causes decrease in damping ratio and Young's modulus.
- Increase in loading frequency cause increase in Young's modulus at low strain in rockfill materials. But the rate of increase in E due to increase of loading frequency decreases at axial strain higher than 0.005%. It seems that E is slightly affected by loading frequency.
- At higher loading frequency (5 Hz), the energy loss may be high, as the integral of drag force between the particles and the displacement may become maximum, causing high damping. Reduction of number of contact surfaces and increasing collision between particles is possible during higher settlement. This may cause higher damping at higher frequency and low confining pressure.
- The anisotropic specimen has considerably higher Young's modulus and slightly less damping ratio in comparison to isotropic samples.
- E mainly depends on the initial vertical stress more than confining pressure, saturation condition, and then loading frequency.
- Among initial vertical stress, confining pressure, saturation condition, and loading frequency, the main influence on D is that of the loading frequency.
- The number of cyclic loadings has some effects on E and D results, especially at axial strain higher than 0.005%. The number of cycles increases E up to a maximum 20% for strain level about 0.05%.
- The rate of increase of excess pore water pressure ratio decreases as confining pressure increases. The excess pore pressure at anisotropy condition is less than of the isotropy condition. The values of generated excess pore water pressure in cyclic loading are less dependent on loading frequency, and more dependent on imposed strain level.
- At certain strain in dry anisotropic specimen, the permanent axial displacement increases as loading frequency increases.
- Comparing with spring, the maximum axial displacement ratio is lower for rockfill and not constant with loading frequency, reaching the maximum for frequencies between 1 and 2 Hz.
- When applied cycle number is limited, Marsal Breakage Index (B_g) is mostly dependent on strain level application.
- Finally, selection of the appropriate E and D curves measured at frequency and cycle number similar to those of the anticipated cyclic loading on the representative specimens are of paramount importance. Moreover, it is recommended that loading frequency range in ASTM D 3999 be modified to 5 Hz as upper limit for near fault earthquakes.

Acknowledgments

The research was supported by BHRC under grant 1-1775 (2008). The authors are thankful for the technical help and assistance provided by respected colleagues at the Geotechnical Division of BHRC.

References

[1] Treloar, L.R.G., *The Physics of Rubber Elasticity*, Claredon Press, Oxford (1975).
[2] Burtscher, S., Dorfmann, A. and Bergmeister, K. "Mechanical aspects of high damping rubber", *2nd Int. Ph.D. Symposium in Civil Engineering*, Budapest, pp. 1–7 (1998).
[3] Muhr, A.H. "Mechanical properties of elastomeric base isolators", *10th European Conference on Earthquake Engineering*, Duma (1995).
[4] Indraratna, B., Ionescu, D. and Christie, H.D. "Shear behavior of railway ballast based on large-scale triaxial tests", *Journal of Geotechnical and Geoenvironmental Engineering, ASCE*, 124(5), pp. 439–449 (1998).
[5] Varadarajan, A., Sharma, K.G., Venkatachalam, K. and Gupta, A.K. "Testing and modeling two rockfill materials", *Journal of Geotechnical and Geoenvironmental Engineering, ASCE*, 129(3), pp. 206–218 (2003).
[6] Ghanbari, A., Sadeghpour, A.H., Mohamadzadeh, H. and Mohamadzadeh, M. "An experimental study on the behavior of rockfill materials using large scale tests", *Electronic Journal of Geotechnical Engineering*, 13(Bundle G), pp. 1–16 (2008).
[7] Aghaei Araei, A., Soroush, A. and Rayhani, M.H.T. "Testing and numerical modeling of rounded and angular rockfill materials", *Scientia Iranica*, 17(3), pp. 169–183 (2010).
[8] Seed, H.B., Wong, R.T., Idriss, I.M. and Tokimatsu, K. "Moduli and damping factors for dynamic analyses of cohesionless soils", *Journal of Geotechnical Engineering*, 112(11), pp. 1016–1032 (1986).
[9] Shibuya, S., Kong, X.J. and Tatsuoka, F. "Deformation characteristics of gravels subjected to monotonic and cyclic loading", *Proceedings of the 8th Japan Earthquake Engineering Symposium*, 1, pp. 771–776 (1990).

[10] Goto, S., Nishio, S. and Yoshimi, Y. "Dynamic properties of gravels sampled by ground freezing", In *Ground Failure Under Seismic Conditions*, S. Prakash and P. Dakoulas, Eds., In *ASCE Geotechnical Special Publication*, 44, pp. 141–157, (1994).

[11] Kokusho, T. and Tanaka, Y. "Dynamic properties of gravel layers investigated by in situ freezing sampling", In *Ground Failure Under Seismic Conditions*, S. Prakash and P. Dakoulas, Eds., In *ASCE Geotechnical Special Publication*, 44, pp. 121–140, (1994).

[12] Yasuda, N. and Matsumoto, N. "Comparisons of deformation characteristics of rockfill materials using monotonic and cyclic loading laboratory tests and in situ tests", *Canadian Geotechnical Journal*, 31, pp. 162–174 (1994).

[13] Hatanaka, M. and Uchida, A. "Effects of test methods on the cyclic deformation characteristics of high quality undisturbed gravel samples", In *Static and Dynamic Properties of Gravelly Soils*, In *Geotechnical Special Publication*, 56, pp. 136–151, (1995).

[14] Lin, S., Lin, P.S., Luo, H. and Juang, H. "Shear modulus and damping ratio characteristics of gravelly deposits", *Canadian Geotechnical Journal*, 37, pp. 638–651 (2000).

[15] Hardin, B. and Kalinski, M. "Estimating the shear modulus of gravelly soils", *Journal of Geotechnical and Geoenvironmental Engineering, ASCE*, 131(7), pp. 867–875 (2005).

[16] Aghaei Araei, A., Tabatabaei, S.H. and Ghalandarzadeh, A. "Assessment of shear modulus and damping ratio of gravelly soils", Research Project, No.3-4469-2007, BHRC, Iran (2008).

[17] Aghaei Araei, A., Razeghi, H.R., Tabatabaei, S.H. and Ghalandarzadeh, A. "Evaluation of frequency content on properties of gravelly soils", Research Project, No.1–1775-2008, BHRC, Iran (2009).

[18] Aghaei Araei, A., Razeghi, H.R., Tabatabaei, S.H. and Ghalandarzadeh, A. "Dynamic properties of gravelly materials", *Scientia Iranica*, 17(4), pp. 245–261 (2010).

[19] Aghaei Araei, A., Razeghi, H.R., Tabatabaei, S.H. and Ghalandarzadeh, A. "Loading frequency effect on stiffness, damping and cyclic strength of modeled rockfill materials", *Soil Dynamics and Earthquake Engineering*, 33, pp. 1–18 (2012), http://dx.doi.org/10.1016/j.soildyn.2011.05.009.

[20] Aghaei Araei, A., Tabatabaei, S.H. and Razeghi, H.R. "Cyclic and post-cyclic monotonic behavior of crushed conglomerate rockfill material under dry and saturated conditions", *Scientia Iranica, Transaction of A: Civil Engineering*, 19(1), pp. 64–76 (2012), http://dx.doi.org/10.1016/j.scient.2011.12.001.

[21] Khan, Z.H., Cascante, G., El Naggar, M.H. and Lai, C.G. "Measurement of frequency-dependent dynamic properties of soils using the Resonant-Column device", *Journal of Geotechnical and Geoenvironmental Engineering, ASCE*, 134(9), pp. 1319–1326 (2008).

[22] Park, D. and Hashash, Y.M.A. "Rate-dependent soil behavior in seismic site response analysis", *Canadian Geotechnical Journal*, 45(4), pp. 454–469 (2008).

[23] Meng, J. "Earthquake ground motion simulation with frequency-dependent soil properties", *Soil Dynamics and Earthquake Engineering*, 27, pp. 234–241 (2007).

[24] Lai, C.G., Pallara, O., Lo Presti, D.C. and Turco, E. "Low-strain stiffness and material damping ratio coupling in soils", In *Advanced Laboratory Stress–Strain Testing of Geomaterials*, T. Tatsuoka, S. Shibuya and R. Kuwano, Eds., pp. 265–274, Balkema, Lisse, Netherlands (2001).

[25] Shibuya, S., Mitachi, T., Fukuda, F. and Degoshi, T. "Strain-rate effects on shear modulus and damping of normally consolidated clay", *Geotechnical Testing Journal*, 18(3), pp. 365–375 (1995).

[26] Sugito, M., Goda, H. and Masuda, T. "Frequency-dependent equ-linearized technique for seismic response analysis of multi-layered ground", *Proceedings of JSCE*, No.493/III-27, pp. 49–58 (in Japanese) (1994).

[27] Sugito, M. "Frequency-dependent equivalent strain for equi-linearized technique", In *Proceedings of the First International Conference on Earthquake Geotechnical Engineering, 1*, pp. 655–660, A.A. Balkena, Rotterdam, Netherlands (1995).

[28] Kwak, D.Y., Jeong, C.G., Park, D. and Park, S. "Comparison of frequency-dependent equivalent linear analysis methods", *The 14th World Conference on Earthquake Engineering*, Beijing, China, p. 8 (October 12–17 2008).

[29] Yoshida, N., Kobayashi, S., Suetomi, I. and Miura, K. "Equivalent linear method considering frequency dependent characteristics of stiffness and damping", *Soil Dynamics and Earthquake Engineering*, 22(3), pp. 205–222 (2002).

[30] Assimaki, D. and Kausel, E. "An equivalent linear algorithm with frequency and pressure-dependent moduli and damping for the seismic analysis of deep sites", *Soil Dynamics and Earthquake Engineering*, 22, pp. 959–965 (2002), http://dx.doi.org/10.1016/S0267-7261(02)00120-3.

[31] Zeghal, M., Elgamal, A.W., Tang, H.T. and Stepp, J.C. "Lotung downhole array II: evaluation of soil nonlinear properties", *Journal of Geotechnical Engineering, ASCE*, 121(4), pp. 363–378 (1995).

[32] Kokusho, T., Aoyagi, T. and Wakunami, A. "In-situ soil-specific nonlinear properties back-calculated from vertical array records during 1995 Kobe earthquake", *Journal of Geotechnical and Geoenvironmental Engineering, ASCE*, 131(11), pp. 1509–1521 (2005).

[33] Sundarraj, K.P. "Evaluation of deformation characteristics of 1-G model ground during shaking using a laminar box", Ph.D. Dissertation, University of Tokyo, Japan (1996).

[34] Kallioglou, P., Tika, T.H. and Pitilakis, K. "Shear modulus and damping ratio of cohesive soils", *Journal of Earthquake Engineering*, 12, pp. 879–913 (2008).

[35] Rollins, K.M., Evans, M.D., Diehl, N.B. and Daily, W.D. "Shear modulus and damping relationships for gravels", *Journal of Geotechnical and Geoenvironmental Engineering, ASCE*, 124(5), pp. 398–405 (1998).

[36] Feizi-Khankandi, S., Mirghasemi, A.A., Ghalandarzadeh, A. and Hoeg, K. "The cyclic triaxial tests on asphalt concrete as a water barrier for embankment dams", *Soils and Foundations*, 48(3), pp. 319–332 (2008).

[37] ASTM Standard D3999-91. "Standard test methods for the determination of the modulus and damping properties of soils using the cyclic triaxial apparatus", In *Annual Book of ASTM Standard*, ASTM International, West Conshohocken, PA (2003).

[38] Tiedemann, D.A., Kaufman, L.P. and Rosenfield, J. "Determining dynamic properties for embankment dams from laboratory testing", Report No. REC-ERC- 84–17, US Department of Interior, Bureau of Reclamation, Denver CO, p. 34 (December 1984).

[39] Aghaei Araei, A. "Back analysis of deformations induced during first impounding of Masjed-e-Soleyman dam", M.Sc. Thesis, Department of Civil and Environmental Engineering, Amirkabir University of Technology, Tehran, Iran (2002).

[40] Jiang, G.L., Tatsuoka, F., Flora, A. and Koseki, J. "Inherent and stress-state-induced anisotropy in very small strain stiffness of a sandy gravel", *Geotechnique*, 47(3), pp. 509–521 (1997).

[41] Kokusho, T. "Cyclic triaxial test of dynamic soil properties for wide strain range", *Soils and Foundations*, 20, pp. 45–60 (1980).

[42] Tatsuoka, F. and Shibuya, S. "Deformation characteristics of soils and rock from field and laboratory tests", In *9th Asian Regional Conference on SMFE*, In *Keynote Lecture*, 1.2, pp. 101–170, Bangkok (1992).

[43] Tatsuoka, F., Kohata, Y. and Lo Presti, D. "Deformation characteristics of soils and soft rocks under monotonic and cyclic loads and their relationships", *Proceedings: Third International Conference on Recent advances in Geotechnical Earthquake Engineering and Soil Dynamics*, Paper No. SOA1, Volume II, St. Louis, Missouri, pp. 851–879 (April 2–7 1995).

[44] Tatsuoka, F., Teachavorasinskun, S., Dong, J., Kohata, Y. and Sato, T. "Importance of measuring local strains in cyclic triaxial tests on granular materials", *ASTM STP*, 1213, pp. 288–302 (1994).

[45] Thomson, W.T. and Dahleh, M.D., *Theory of Vibration with Applications*, 5th Edn., Prentice Hall, USA, pp. 23–24 (1998).

[46] Chopra, A.K., *Dynamics of Structures: Theory and Applications to Earthquake Engineering*, 4th Edn., Prentice Hall, University of California Berkeley (2007).

[47] Aghaei Araei, A. "Effects of different parameters on dynamic behavior of compacted rockfill materials using large scale triaxial equipment", Ph.D. Thesis, Iran University of Science and Technology, IUST, Iran (2011).

[48] ASTM Standard D1557-02e1. "Standard test methods for laboratory compaction characteristics of soil using modified effort", In *Annual Book of ASTM Standard*, ASTM International, West Conshohocken, PA (2003).

[49] ASTM Standard D4718-03. "Practice for correction of unit weight and water content for soils containing oversize particles", In *Annual Book of ASTM Standard*, ASTM International, West Conshohocken, PA (2003).

[50] ASTM Standard D4767-04. "Standard test method for consolidated undrained triaxial compression test for cohesive soils", In *Annual Book of ASTM Standard*, ASTM International, West Conshohocken, PA (2004).

[51] ASTM Standard D5311-92. "Standard test method for load controlled cyclic triaxial strength of soil", In *Annual Book of ASTM Standard*, ASTM International, West Conshohocken, PA (2004).

[52] Kramer, S.L., *Geotechnical Earthquake Engineering*, Prentice Hall, Upper Saddle River, New Jersey (1996).

[53] ASTM Standard D4015-1992. "Standard test methods for modulus and damping of soils by the resonant-column method", In *Annual Book of ASTM Standard*, ASTM International, West Conshohocken, PA (2000).

[54] Marsal, R.J. "Large scale testing of rockfill materials", *Journal of the Soil Mechanics and Foundations Division, ASCE*, 93(SM2), pp. 27–43 (1967).

[55] Gupta, A.K. "Effect of particle size and confining pressure on breakage and strength parameters of rockfill materials", *Electronic Journal of Geotechnical Engineering*, 14(Bund. H), pp. 1–12 (2009).

[56] Towhata, I., *Geotechnical Earthquake Engineering*, Springer (2008).

[57] Aziz, M. "Experimental study on effects of deterioration of grains on deformation and strength characteristics of soils", Ph.D. Thesis, Department of Civil Engineering, The University of Tokyo, Japan (2010).
[58] Towhata, I. and Aghaei Araei, A. "Assessment of the GAP-SENSOR use for measuring dynamic behaviors of geomaterials", Unpublished Results, The University of Tokyo, Japan (2010).

Ata Aghaei Araei received his Ph.D. from Iran University of Science and Technology (IUST), Iran, in 2011. He also was Ph.D. Researcher at the Geotechnical Laboratory of Civil Engineering at The University of Tokyo. He is a faculty member of the Road, Housing and Urban Development Research Center (BHRC) in Iran where, since 2003, he has been working as Senior Geotechnical Engineer and Head of the Geotechnical Laboratory. Dr. Aghaei Araei's primary research interests include: Monotonic and Dynamic Testing on Geomaterials, Microzonation, and Geotechnical Equipment Construction.

Hamid Reza Razeghi received his Ph.D. from Tohoku University, Japan, in 2000 and he is currently an Assistant Professor in the School of Civil Engineering at Iran University of Science and Technology, in Iran. His research interests include: Geotechnical and Geoenvironmental Engineering.

Abbas Ghalandarzadeh is Associate Professor in the School of Civil Engineering at the University of Tehran, where he is also currently Head of the Soil Mechanics and Centrifuge Laboratory. He received his Ph.D. degree in Geotechnical Engineering from the University of Tokyo in 1997. He is a member of the Technical Committee of TC2 of the International Society of Soil Mechanics and Geotechnical Engineering. His research interests are mainly in the area of Experimental Geotechnics, particularly in model and element testing. Dr. Ghalandarzadeh has undertaken much research in the area of Earthquake Geotechnical Engineering including: the Dynamic Behavior of Rockfill Dams with Asphalt Concrete Cores, the Seismic Behavior of Quay Walls, Reinforced Earth and Piles, and more recently the Anisotropic Behavior of Saturated Sands Mixed with Clay or Silt.

Saeid Hashemi Tabatabaei received his Ph.D. from Roorkee University, India, in 1992. He is a faculty member of the Road, Housing and Urban Development Research Center (BHRC) in Iran where, since 2002, he has been Head of the Geotechnical Department. He has over 18 years of experience in the field of geotechnical engineering and geotechnical engineering research. He has been involved in over 33 engineering projects in the fields of Landslide Hazard and Risk Assessment, Slope Stability Analysis and Mitigation, Soil Improvement, Engineering Geological Mapping for Microzonation of Rural Areas and Site Investigation.